Thermal runaway and fire of electric vehicle Li-ion battery and contamination of infrastructure facility

Authors: M. Held, M. Tuchschmid, M. Zennegg, R. Figi, C. Schreiner, L.D. Mellert, U. Welte, M. Kompatscher, M. Hermann, and L. Nachef

Journal: *Renewable and Sustainable Energy Reviews*

Date: Accepted 3 April 2022, Version of Record 21 May 2022

Citation: Volume **165**, 112474, DOI: 10.1016/j.rser.2022.112474

Open Access article, PDF attached.

Renewable and Sustainable Energy Reviews 165 (2022) 112474

Contents lists available at ScienceDirect

Renewable and Sustainable Energy Reviews

journal homepage: www.elsevier.com/locate/rser

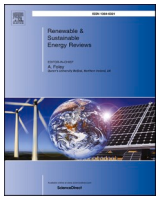

Thermal runaway and fire of electric vehicle lithium-ion battery and contamination of infrastructure facility

Marcel Held [a,*], Martin Tuchschmid [a], Markus Zennegg [a], Renato Figi [a], Claudia Schreiner [a], Lars Derek Mellert [b], Urs Welte [b], Michael Kompatscher [c], Michael Hermann [c], Léa Nachef [d]

[a] Empa, Swiss Federal Laboratories for Materials Science and Technology, Überlandstr. 129, 8600, Dübendorf, Switzerland
[b] Amstein + Walthert Progress AG, Andreasstr. 5, 8050, Zürich, Switzerland
[c] Hagerbach Test Gallery Ltd., Polistrasse 1, 8893, Flums, Switzerland
[d] Centre d'Études des Tunnels, 25 Avenue François Mitterrand, 69500, Bron, France

ARTICLE INFO

Keywords:
Lithium ion battery
Thermal runaway
Fire
Contamination
Toxicity
Chemical analysis

ABSTRACT

Thermal runaway and the subsequent fire of electric vehicle lithium-ion batteries cause a specific type of contamination. In order to assess the resulting risks of damage to critical infrastructure and to human health, we perform practical thermal runaway experiments with lithium-ion battery modules of an approved, commercially available electric vehicle. Extensive chemical analyses identify and quantify the soot depositions in ventilated and non-ventilated rooms. Contamination mainly consists of the metal oxides of the cathode material, lithium and fluoride compounds. Their influence on surfaces, protective textiles as well as their corrosiveness to typical metals and the impairment of electrical and electronic devices is low. The analysis of sprinkling and cooling water shows the necessary extent of its decontamination. Recommendations include preventive and mitigating measures for the appropriate handling of contamination caused by fires from lithium-ion battery powered electric vehicles.

1. Introduction

Battery electric vehicles (BEV) have the potential to substitute vehicles with internal combustion engines and could contribute – at least locally - to a more sustainable transportation sector by the reduction of greenhouse gases (GHG), toxic gases and particle emissions [1–3]. A large part of future mobility will be electrified [4] and will increasingly take place underground, whether driving through tunnels or parking and charging in enclosed spaces. Therefore, the importance of safety and availability of infrastructure facilities are increasing. Fire and explosion risks associated with batteries pose a danger for commercial property, especially if many cars are being charged in underground car parks [5].

The energy supply of today's electric cars is based almost exclusively on lithium ion batteries (LIBs) with various metal oxides as the positive electrode - the cathode - material, graphite as anode material, a liquid electrolyte based on organic carbonates containing a dissociated conducting salt, and a permeable separator between the electrodes. These batteries differ mainly in the cathode materials, where lithium cobalt oxide ($LiCoO_2$, LCO), lithium manganese oxide ($LiMn_2O_4$, LMO), lithium iron phosphate ($LiFePO_4$, LFP), lithium nickel-manganese-cobalt oxide ($LiNiMnCoO_2$, NMC) and lithium nickel cobalt aluminum oxide ($LiNiCoAlO_2$, NCA) are used, each having their specific advantages and disadvantages [6,7]. These metal oxides powders mixed with conductivity enhancers, usually carbon black, and binder materials are coated onto a – usually aluminum – current collector. Batteries for present BEV have capacities of 16–100 kWh for driving ranges from 100 to 600 km [8,9]. NMC, a combination of nickel, manganese and cobalt, is gaining popularity in electric mobility applications mainly due to its high specific energy (Wh/kg) and an acceptable set of parameters concerning safety, cost, power and energy density (W/l, Wh/l), lifetime and temperature stability. The mixing ratio of Ni, Mn an Co tends to nickel rich compounds for higher energy density and reduction of cobalt content [10–12] and exists in varieties such as NMC (1:1:1), NMC (5:3:2), NMC (6:2:2) and NMC (8:1:1) commercialized in EV applications by Nio and CATL in 2019 [13].

The lithium-ion cell negative electrode, the anode, is composed of a lithium intercalation compound coated onto a metal - usually copper - current collector. The most common anode material is a form of graphite

* Corresponding author.
E-mail address: marcel.held@empa.ch (M. Held).

https://doi.org/10.1016/j.rser.2022.112474
Received 22 December 2021; Received in revised form 29 March 2022; Accepted 13 April 2022
Available online 21 May 2022

combined with binder material. There are many different subspecies of graphite anodes, which differ in their origin (natural, synthetic), purity, particle size, particle size distribution, particle shape, particle porosity, crystalline phase, degree of compaction etc.

The liquid electrolyte of all the LIBs usually consists of organic solvents such as ethylene carbonate (EC), dimethyl carbonate (DMC), and diethyl carbonate (DEC) with lithiumhexafluorophosphate ($LiPF_6$) as a conducting salt enabling the shuttle transport of lithium cations (Li^+) between anode and cathode.

This combination of anode and cathode material plus electrolyte enables the high energy densities required for batteries in electric cars reaching from 120 Wh/kg (LFP), 220 Wh/kg (NMC) up to 250 Wh/kg (NCA) on a cell level. However, this chemistry poses a considerable safety problem mainly due to the flammable electrolyte but also because exothermic decomposition reactions of anode and cathode materials can be triggered in case of a fault of the battery [14]. An overview of failure modes, mechanisms, and effects analysis (FMMEA) of LIBs that can lead to fire is given by Hendricks et al. [15].

1.1. Thermal runaway and its consequences

The effect of failing LIBs is often a so-called thermal runaway characterized by an exponential increase of the temperature inside the cell so that the rate of heat generation becomes faster than the rate of heat removal. This leads to an increase of cell internal pressure causing the opening of overpressure devices or bursting of the cell housing. As a result, hot, flammable gases escape and a fire starts. Because cells are densely packed, thermal runaway of one cell is likely to propagate to neighboring cells and eventually setting the whole battery on fire. The theory of thermal runaway and propagation of lithium-ion batteries is well understood and described in many practical investigations [16–20].

The composition of exiting gases and substances as well as temperatures of various LIB types in thermal runaway have also been investigated. However, these findings are not always consistent and can show considerable variation.

Some studies have determined the composition and volume of the partially flammable gases produced during the thermal runaway of commercial battery cell types, e.g. NMC, LCO, LFP, LMO [21–24]. These studies found concentrations of 5–30% of H_2, 5–30% of CO, 20–90% of CO_2 and 0–9% of various hydrocarbons (methane, ethene, propene, ethane, butene, propane, butane), whereas variation of concentrations is related to different state of charge (SOC) of the investigated cells.

The comprehensive report of the Research Centre for Fire Protection Technology of the Karlsruhe Institute of Technology [25] describes the various compositions of LIBs and theoretically possible chemical reactions during thermal runaway. A fire test with a lithium-ion vehicle battery (size and type not specified) found irritant, toxic, polycyclic aromatic hydrocarbons (PAHs) which are environmental and water pollutants, as well as, in part, toxic concentrations of heavy metals. Dioxins, furans and phosgene were not detected. A substantial proportion of the literature refers to the analysis of the chemical decomposition during the combustion of the electrolyte, the conducting salt $LiPF_6$ or a combination thereof [26,27]. Among the toxic substances generated during combustion hydrofluoric acid gas (HF) is a major concern. In Ref. [27], a quantity of 18–60 mg of HF gas per gram of electrolyte mixture is specified for the combustion of electrolyte mixtures with $LiPF_6$ conducting salt.

Such values represent rather the maximum of the expected generation of HF, because in the combustion of complete cells, lower quantities were found than could be extrapolated based on the electrolyte content. For example, Ribière et al. [28] found 36–68 mg of HF per Wh for an LMO pouch cell with nominal electrical energy 2.9 Ah/11 Wh. Larsson et al. [29] measured HF concentrations during combustion of LFP, LCO and NCA cells and derived a generation of 20–200 mg HF per Wh of nominal energy. Lecocq et al. [30] measured a HF mass flux of 1–4 mg/s for about 200 s during combustion of 1.3 Ah/4.2 Wh LFP pouch cells, yielding 50 mg/Wh for cells at 100% SOC and 105 mg/Wh for 0% SOC. Sun et al. [31] show a relative comparison of the quantities of HF and phosphoruos oxides (POx) during the combustion of commercial cells (LMO, NMC, LFP, LCO) and finds a large number of other acutely toxic substances, although no quantities are given.

Comparisons of BEV and internal combustion engine (ICE) vehicle fires show that the maximum heat release rate, the overall dissipated heat of combustion and the effective heat of combustion are close for both types of vehicles [32,33]. Moreover, Lecocq [32] showed that similar amounts of combustion gases CO_2, CO, total hydrocarbons, NO, NO_2, HCl and HCN are generated by BEV and ICE vehicle fires. BEV fires, however, produce about twice the amount of HF. Mellert et al. [34] found critical concentrations of the two heavy metals cobalt and manganese as well as lithium in the form of aerosols after combustion of NMC battery modules. However, they conclude that no impairment should be expected in well-ventilated road tunnels. We can therefore conclude that the potential thermal effects and emissions during lithium-ion battery fires are generally known. Nevertheless, the effects of BEV fires and the subsequent contamination of technical facilities in enclosed spaces remain unclear. This is also due to the lack of fire statistics at the international level for LIB incidents as pointed out by Bravo Diaz et al. [35]. Blum and Long [36] also notice the lack of post-fire incident response and recovery procedures. This study therefore as outlined in the project report [37] focuses on analyzing the remaining contamination after a battery fire in an enclosed space and estimating its potential damage to technical infrastructure and sprinkling or storage water.

2. Experimental setup

2.1. Test sites

The experiments focused on the so-called ‘cold fire site’, defined as the area of damage in which, after the fire has been extinguished or went out by itself and the burned material has cooled down to ambient temperature, the fire residues have settled on the surfaces in the form of soot. Therefore, only analyses of fire residues were carried out and no gas analyses during battery fire. For a target-oriented, safe and environmentally sound execution of the tests, two different environmental profiles were required. One test site with a clearly defined spatial volume of 250 m^3 - test site A - for the analysis of contaminations in a closed environment without air circulation, and another test site with a long measuring section to examine the transport and deposition behavior of the battery-specific fire emissions, test site B.

2.2. Tested battery modules

Tests focused on high-capacity batteries for popular mid-range passenger BEVs. The battery modules used in the experiments were new (produced in 2018) and fully serviceable components of a commercial BEV, parameters are given in Table 1. Such a module represents 1/8 of the complete BEV battery system. Prior to the experiments, modules were charged according to manufacturer’s specification to 100% SOC.

Table 1
Characteristics of the investigated lithium-ion battery module.

Parameter	Battery module
Number of cells	12
Cell type	Prismatic, 90 Ah, Samsung SDI
Anode material	Graphite
Cathode material	$LiNiMnCoO_2$ (NMC 111)
Electrolyte	Organic carbonates
Conducting salt	$LiPF_6$
Nominal voltage	44 V (3.68 V per cell)
Energy	4.15 kWh
Specific energy	0.14 kWh/kg

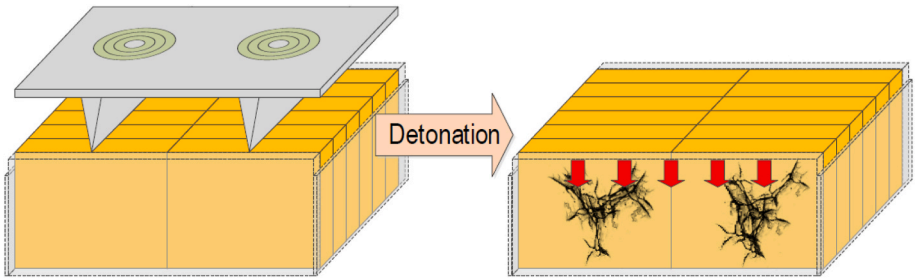

Fig. 1. Battery module (orange) and overlying steel plate with wedges (grey) with detonating fuse (green) before and after application of force (red).

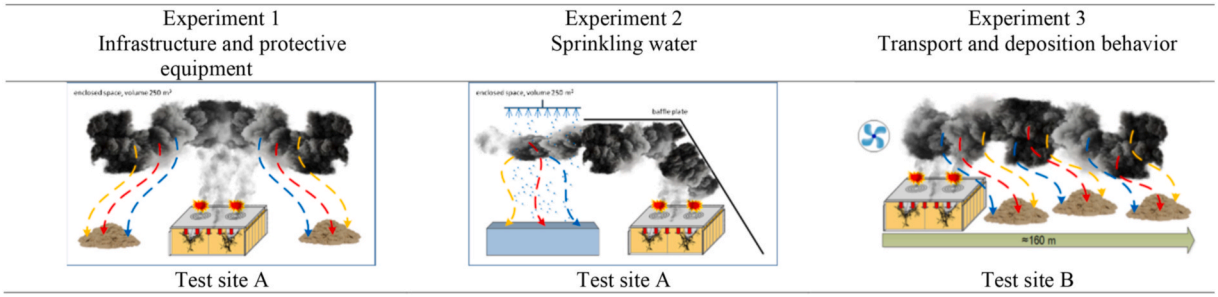

Fig. 2. Illustration of the three test scenarios.

SOC of 100% is set because it represents the worst fire scenario for battery in risk assessment. This is mainly because thermal runaway at high SOC produces more gases, the gases are more flammable and the heat release rate is maximum, see Refs. [14,17,22,28–30,33]. Hu [38] shows the importance of accurate SOC and state of health monitoring (SOH) for the safety assessment of batteries.

2.3. Initiation of thermal runaway

The objective of all test scenarios was the simultaneous damaging of all battery cells in order to cause a thermal runaway of the complete module. Therefore, a steel plate (38 cm × 27 cm x 2 cm) with two 8-cm-long sharpened steel wedges (8 cm × 25 cm x 0.8 cm) running the entire length of its underside was loosely placed atop the battery module, which was attached to the ground, see Fig. 1. Two 100 g bundles of detonating fuse (Detonex, 40 g/m) were affixed to the upper side of the steel plate. Through the simultaneous detonation of both blasting charges, the steel plate was accelerated down into the battery module. The wedges penetrated all 12 cells and caused short-circuiting.

2.4. Test scenarios

To examine potential secondary damage caused by battery fire in underground traffic infrastructures, three battery modules were tested in three experiments illustrated in Fig. 2.

2.4.1. Experiment 1, infrastructure and protective equipment

The goals of this scenario are the quantitative chemical analysis of toxicologically relevant contamination on surfaces and textile protective equipment, the impact of residues on electronic equipment as well as the corrosiveness to typical metals. To allow scaling of the contamination measurements to the vehicle level, the experimental spatial volume was chosen proportional to the energy capacity of the battery module: 1/8 of a battery system → 1/8 of a parking floor with approx. 2000 m^3 (28 × 28 × 2.5 m for 30 cars) ≈ 250 m^3. Thermal runaway is initiated on the battery module in this enclosed test site without ventilation and without extinguishing the fire. Thus, the battery module is completely burned down in order to enable a free deposition of fire emissions on surfaces and in devices.

Fig. 3. Test site A.

Test site A is characterized by and equipped with:

- Clearly defined space (≈250 m^3) without mechanical ventilation: The boundary was created on both sides by means of a construction fleece that was freely suspended at the lower edge (expansion possibility) and wetted with water (fire protection), see Figs. 3 and 4
- Tunnel and parking garage-like environment
- Explosion-proof and smoke-insensitive environment
- Chemically inert surfaces

Fig. 4. Position of collector plates, textile, PC, and corrosion metal plates, test site A, experiment 1.

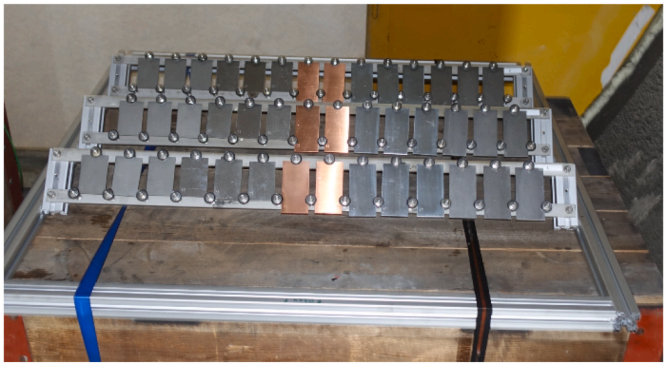

Fig. 5. Rack with corrosion monitoring metal plates.

Fig. 6. Firefighter's textile protective suit.

- Mechanical air purification and smoke evacuation to the outside possible at any time
- Six sample collector plates (2 pieces 50 × 120 cm, 4 pieces 50 × 90 cm, stainless steel 1.4401) at heights of 1 and 3 m, tilted 45° towards experiment, see Figs. 3 and 4
- A rack with corrosion monitoring metal plates at a height of 0.95 m, tilted 45° towards experiment. Metal plates (100 × 50 × 1 mm) are carbon steel, zinc, copper, aluminum alloy AlMgSi1 and stainless steel 1.4404, see Fig. 5
- A firefighter's textile protective suit typically used in such operations consisting of 93% aramid (Nomex), 5% p-aramid (Kevlar), and 2% P140 (carbon), see Fig. 6
- Printed circuit boards in a PC housing with 2 fans for optical inspection and electrical characterization of surface insulation resistance (SIR) before and after test with measuring comb, see Figs. 7 and 8
- Temperature sensors within and around the battery module
- Several lighting devices and video cameras.

Fig. 7. PC housing with printed circuit boards.

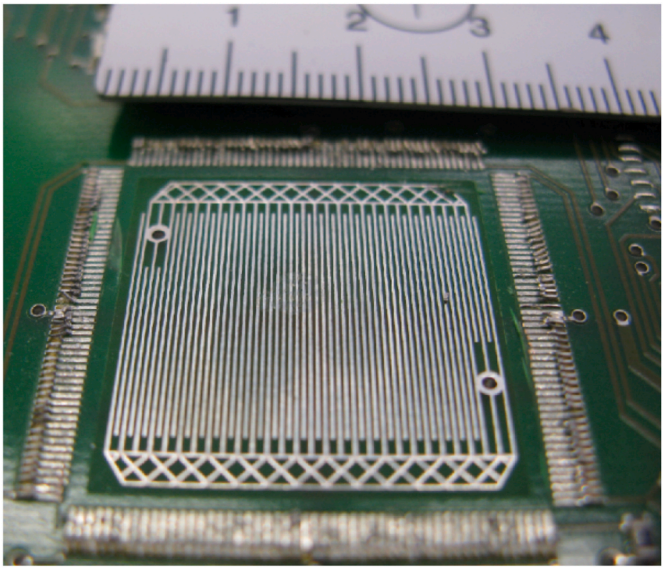

Fig. 8. Measuring comb for surface insulation resistance (SIR) characterization.

2.4.2. Experiment 2, sprinkling and storage water

The goals of this scenario is the quantitative chemical analysis of toxicologically relevant contamination of water that in a real scenario would be generated by the mixture of sprinkling water and smoke emissions of the battery fire. In this scenario, the emissions from the battery fire are sprinkled with a pressure-less water curtain and collected in a large container next to the battery. The battery module itself is not sprinkled and is completely burned down and then stored in a separate container filled with water. Test site A, depicted in Fig. 9, is therefore equipped with:

- Baffle plates on one side and above the battery to direct the fire emissions to the sprinkling zone above the container
- A sprinkler (400 mm × 400 mm) with 324 nozzles at a height of 2.5 m using conventional tap water with a continuous volume flow rate of approximately 20 l/min
- A chemically inert plastic container with a volume of ≈400 l for the collection of all sprinkling water
- A container (570 × 370 × 320 mm) to store the burned down battery in water
- Temperature sensors within and around the battery module
- Several lighting devices and video cameras.

2.4.3. Experiment 3, transport and deposition behaviour

The goal of this experiment is the quantitative chemical analysis of the contaminations that are toxicologically relevant and relevant in terms of chemical corrosion over a longer transport distance. Therefore, a thermal runaway was initiated on the battery module in an open tunnel area - test site B – with a defined airflow (1.5 m/s) and predetermined ventilation route from the fire site through the tunnel into the open air with a length of 160 m. Also in this scenario, the battery module is completely burned down in order to achieve free movement and deposition of all fire emissions along the measuring section. Test site B is characterized by and equipped with:

- Tunnel and parking garage-like environment with long measuring distance (approx. 160 m)
- Explosion-proof and smoke-insensitive environment
- Chemically inert surfaces
- Constant airflow of approx. 1.5 m/s
- Ventilation control and smoke discharge to the open air possible at any time
- Sets of collector plates (1 piece 50 × 120 cm, 2 pieces 50 × 90 cm, stainless steel 1.4401) at a height of 3.5 m, tilted 45° against the air flow. Sets were placed at distances of 50, 100 and 150 m from the battery fire, see Fig. 10
- Temperature sensors within and around the battery module
- Several lighting devices and video cameras.

2.5. Analysis concept

Investigation was focused on the so-called ‘cold fire site‘, therefore only analyses of fire residues were carried out instead of gas analyses during the fires. The latter were the focus of a previous investigation and are documented in Mellert et al. [34]. Those measurements indicated that BEV fires resulted in changed chemical hazards and contaminations in comparison to conventional vehicle fires. Only inspected measuring equipment and devices that were within the calibration cycle specified by the manufacturer were used during the tests. The ambient conditions on site were recorded and documented with suitable measuring equipment before and during each test. The basic analysis and measurement methods used for the individual parameters are shown in Table 2. Details are given in the experiment analysis concept in the annex.

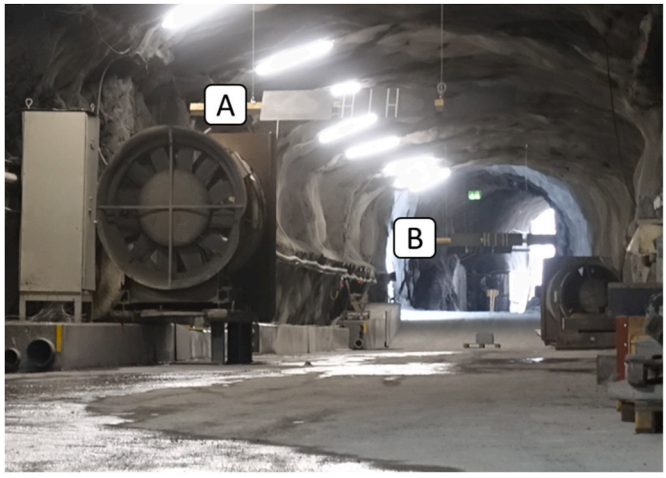

Fig. 10. Fan and collector plates at 100 m (A) and 150 m (B) in tunnel of test site B.

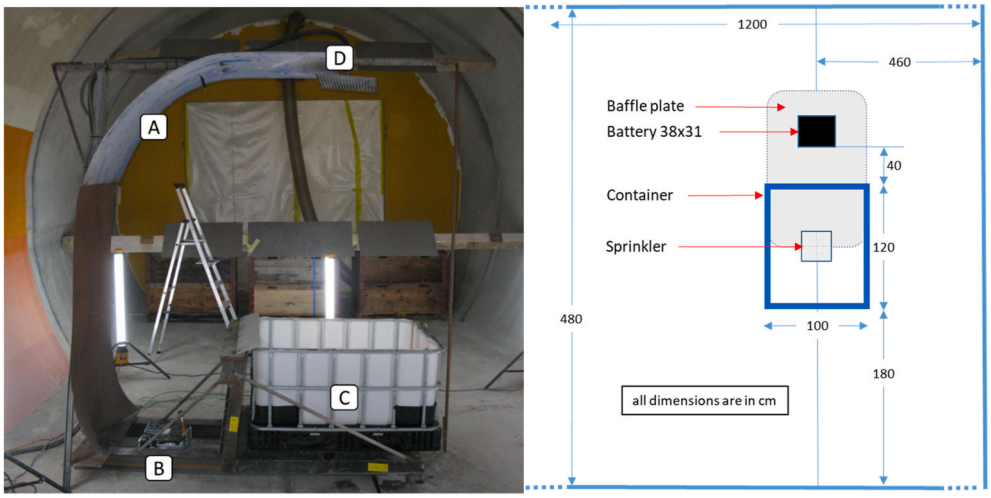

Fig. 9. Position of baffle plate (A), battery (B), collection container (C), and sprinkler (D), test site A, experiment 2.

Table 2
Measured parameters/substances and methods.

Measured parameter/substance	Description	Analysis/measurement method
Temperature	Temperature in the direct vicinity and inside the battery module	Direct, with type K thermocouples
F^-, Cl^-, Br^- Anions, Cations	Contamination with halogens (particularly hydrofluoric acid HF) and anions, cations	Surface swipe samples: anion analysis in aqueous extract through capillary electrophoresis (CE). Water samples: direct CE anion and cation analysis
$HCOO^-$, CH_3COO^-	Contamination with formic and acetic acid	
SO_4^{2-}, NO_3^-, PO_4^{3-}	Contamination with sulphuric, nitric and phosphoric acid	
Li, Ni, Co, Mn	Contamination with lithium, nickel, cobalt and manganese compounds	Quantitative determination of mass concentrations in µg/cm² (surface swipe samples, acidulated) and mg/l (water samples, acidulated), mass fractions in g/100 g (soot, filtrate of waters samples) of Co, Li, Mn and Ni by inductively coupled plasma optical emission spectrometry ICP-OES.
PAH, PCB, PCDD/F	Contamination with polycyclic aromatic hydrocarbons, polychlorinated biphenyls and polychlorinated dibenzodioxins/furans	Surface swipe samples: analysis in cyclohexane or toluene extract through gas chromatography and high-resolution mass spectrometry, GC-HRMS Water samples: n-hexane extract from C18 phase or polymer cartridge, isotope dilution analysis, GC-HRMS.
Element screening	Analysis of the overall chemical composition of the fire soot samples	Semi quantitative element analysis using SEM-EDX and energy dispersive X-ray fluorescence, ED-XRF.
Smoke generation	Intensity and chronological sequence of smoke generation	Direct, with video (high-resolution recordings [1080p] with normal frame rate [30 fps]).
Pressure effects	Deflagration, explosion	
Corrosiveness of contamination	Analysis of corrosion damage to various typical infrastructure metals	Gravimetric analysis of corrosion induced mass loss on exposed test plates: directly after exposure of the test plates to smoke gases (and decontamination) after exposure of the contaminated test plates at 90% relative humidity (for a period of 3 months).
Electrical conductivity and electrochemical characteristics	Impact of contamination on electronic components on printed circuit board and on contaminated water	Soot: measurement of surface insulation resistance SIR before and after contamination, direct measurement of soot conductivity under mechanical pressure. Water samples: pH-value and electrical conductivity.

3. Results

3.1. Results infrastructure and protective equipment

The fire soot quantities on the collector plates in the test tunnel measured gravimetrically are at 17–20 g/m². Orienting SEM-EDX analysis determined that the elements Co, Ni, Mn made up around 20–25% by mass and O was detected with a concentration of 15–20%. The elements Al, C, F and P made up 1–5% by mass, see Table 3. With ICP-OES analysis of the nitric acid extract of the fire soot depositions, the elements Co, Ni an Mn made up around 17–18% by mass and Li was detected at a concentration of around 3% by mass, see Table 4. The elements Co, Ni, Mn were measured to make up 18–20% by mass using ED-XRF. This also shows a good agreement of the analysis and measurement methods, especially of ICP-OES with ED-XRF.

3.1.1. Contamination of infrastructure and textiles

Inorganic pollutants which are toxicological and corrosion chemical relevance were present in the form of large amounts of the elements Co, Ni and Mn, each amounting to approximately 150–400 µg/cm², and of the element Li amounting to around 30–70 µg/cm² , see Table 5. Water-soluble fluorides in amounts of 40–52 µg/cm² were detected on the collector plates and textile, see Table 6. Therefore, the usual background levels for non-contaminated surfaces are exceeded by factors up to approximately 2000–4000 (Co, Ni), 500–700 (Mn), 400–700 (Li) and 50 (fluorides).

Other anions (Bromide Br^-, Sulfate SO_4^{2-}, Nitrate NO_3^-, Formate $HCOO^-$, Acetate CH_3COO^-) and cations (Ammonium NH_4^+, Potassium

Table 5
Cobalt, Nickel, Manganese and Lithium contamination and background values (surface swipe samples, nitric acid extract and ICP-OES), all values in µg/cm², sampling area 200 cm².

Designation	Sample Id.	Nickel	Cobalt	Manganese	Lithium
Collector plate, at 3 m	A-12	234	233	221	42
Collector plate, at 1 m	B-12	156	155	148	30
Textile	T-12	400	400	380	70
Textile, after cleaning	TR-12	<0.3	<0.2	<0.4	<0.5
Collector plate, at 1 m, background	0W-A	<0.3	<0.2	<0.4	<0.5
Textile, background	0T-A	0.5	0.5	0.5	<0.5

Table 3
Fire soot samples, quantities and element analysis with SEM-EDX, sampling area 8000 cm².

Designation	Sample Id.	Quantity	Composition, both samples	
Collector plates, at 3 m	A-2	17 g/m²	Co, Ni, Mn	each 20–25% w/w
Collector plates, at 1 m	B-2	20 g/m²	O	15–20% w/w
			Al, C, F, P	each 1–5% w/w
			Si, Ca, S, Cl	<1% w/w

Table 4
Content of metals in fire soot swipe samples by ICP-OES analysis (method A, % by mass), sampling area 200 cm² and direct analysis of soot with ED-XRF (*method B*, % by mass, mean value of triple measurement ± rounded up standard deviation), sampling area 8000 cm².

Designation	Sample Id.	Nickel		Cobalt		Manganese		Lithium
		A	*B*	A	*B*	A	*B*	A
Collector plate, at 3 m	A 12, *A-2*	17.4	*18.1 ± 0.5*	17.7	*18.2 ± 0.5*	17.1	*19.6 ± 0.5*	3.2
Collector plate, at 1 m	B 12, *B-2*	17.3	*18.6 ± 0.5*	17.7	*18.6 ± 0.5*	17.1	*19.9 ± 0.5*	3.2

Table 6
Anion and Lithium cation contamination (surface swipe samples, aqueous extract and CE), all values in µg/cm^2, sampling area 200 cm^2.

Designation	Sample Id.	Chloride Cl^-	Fluoride F^-	Phosphate PO_4^{3-}	Lithium Li^+
Collector plate 3 m	A-11	5.2	40	2.1	17
Collector plate 1 m	B-11	6.4	52	2.2	23
Textile	T-11	5.3	46	0.8	9.0
Textile after cleaning	TR-11	1.5	bdl	bdl	bdl
Collector plate 1 m, background	0W–K	0.1	bdl	bdl	bdl
Textile, background	0T-K	1.5	bdl	bdl	bdl

Table 7
Contamination with organic pollutants (surface swipe samples, Sohxlet extract and GC-HRMS), sampling area 1000 cm^2.

Designation	Sample Id.	PAH Σ16 EPA-PAH µg/m^2	PCB Σ 6 cong. Ballschmiter x 5 µg/m^2	PCDD/PCDF Σ I-TEQ ng/m^2
Collector plate 3 m	A-13, *A-14*	269	*0.22*	*6.3*
Collector plate 1 m	B-13, *B-14*	304	*9.6*	8.4
Textile	T-13, *T-14*	120	*0.26*	*3.4*
Textile, after cleaning	TR-13, *TR-14*	5.6	*0.17*	*0.3*
Collector plate 1 m, background	0W–O1, *0W–O2*	6.0	*0.36*	*0.2*
Textile, background	0T-O1, *0T-O2*	6.0	*0.8*	*0.2*
Restoration goal [a]		<100	« 100	<50

[a] [39] VdS 2357 - Richtlinien zur Brandschadensanierung (Fire damage restoration guidelines).

K^+, Sodium Na^+, Magnesium Mg^{2+}, Calcium Ca^{2+}) were in amounts below the detection limit (bdl) of the respective method (<0.1 µg/cm^2) or smaller than background values measured pre experiment. Textile sample TR-11 was measured after one ordinary washing cycle.

Toxicologically relevant organic pollutants were observed as slightly elevated PAH quantities of approximately 250–300 µg/m^2, detected on collector plates and 120 µg/m^2 on textiles, which exceeded the measured background levels for non-contaminated surfaces by factors up to approximately 50 and 20, respectively, see Table 7. The level of contamination with PAH is therefore up to a factor of 3 higher than the restoration goal for industrial environments [39]. The PCB and PCDD/F quantities of ≤10 µg/m^2 (PCB) and ≤10 ng/m^2 (PCDD/F) are within the normal range for background levels of non-contaminated surfaces and well below restoration goal (see Table 7).

3.1.2. Corrosion monitoring

The corrosion metal plates were examined for the first time after three days under ambient conditions and after one and three months of storage at room temperature and 90% relative humidity to assess the corrosion induced mass loss. The mass loss rate due to corrosion is determined via gravimetric measurements.

Table 8
Corrosion induced mass loss in g/m^2.

Material	Material No.	Stored at test site for 3 days	Stored at 90% relative humidity	
			after 1 month	after 3 months
Unalloyed steel	1.0660	4.3	23	37
Zinc 99.9%	–	1.8	4.4	7.3
Copper 99.9%	–	0.3	0.4	0.4
Aluminum alloy AlMgSi1	3.2315	0.2	0.2	0.2
Stainless steel	1.4404	0.1	0.1	0.1

The corrosiveness of the fire gas condensates produced during the battery fire can be assessed as insignificant overall and summarized as follows: the test metals unalloyed steel and zinc show only very low mass loss after 3 months of exposure to 90% relative humidity, which is comparable to the mass loss of metals contaminated by a chloride exposure of 5 µg/cm^2 and exposed to 90% relative humidity for 3 months. No corrosion induced mass loss was detected on the test metals copper, aluminum and stainless steel after 3 months of exposure at 90% relative humidity, see Table 8.

3.1.3. Impact on electronics

Content of elements Ni, Mn and Co in soot on printed circuit boards determined with ED-XRF, see Table 9, is in the same range as in soot of collector plate samples shown in Table 4.

All printed circuit boards and the SIR single measuring comb were covered with a thick layer of soot, see Figs. 11 and 12. SEM/EDX analysis primarily showed the heavy metals nickel, cobalt and manganese, Fig. 13, as well as larger quantities of carbon and oxygen.

The measurements of the insulation resistances with a voltage of 500 VDC on all samples showed that the soot deposits did not lead to any conductive paths on the measuring comb. Conductivity of soot under mechanical pressure, Fig. 14, is even smaller than that of pristine NMC as a reference (reference: Sigma Aldrich, $LiNi0.33Mn0.33Co0.33O_2$, CAS Nr. 346417-97-8), see Fig. 15. The low conductivity is an indication

Table 9
Content of metals in fire soot samples collected on printed circuit boards and NMC reference (ED-XRF, % by mass, mean value of 5-fold measurement ± rounded up standard deviation).

Nickel		Cobalt		Manganese	
soot	Ref	soot	Ref	soot	Ref
19.8 ± 0.2	18.3 ± 0.2	19.8 ± 0.2	19.9 ± 0.2	21.2 ± 0.2	25.9 ± 0.2

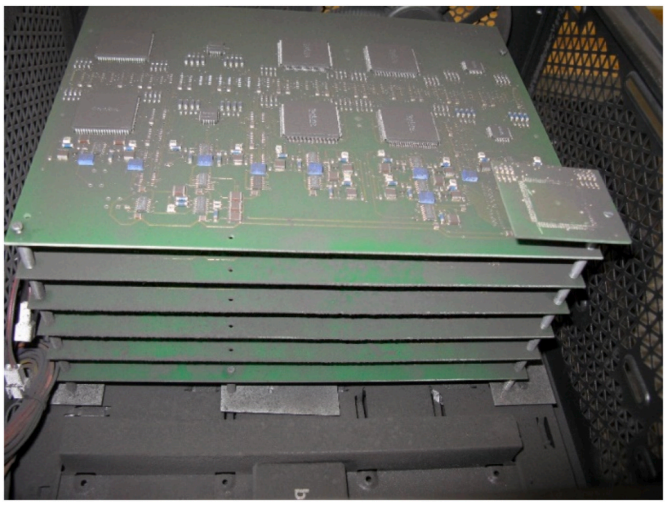

Fig. 11. Soot on printed circuit boards in PC.

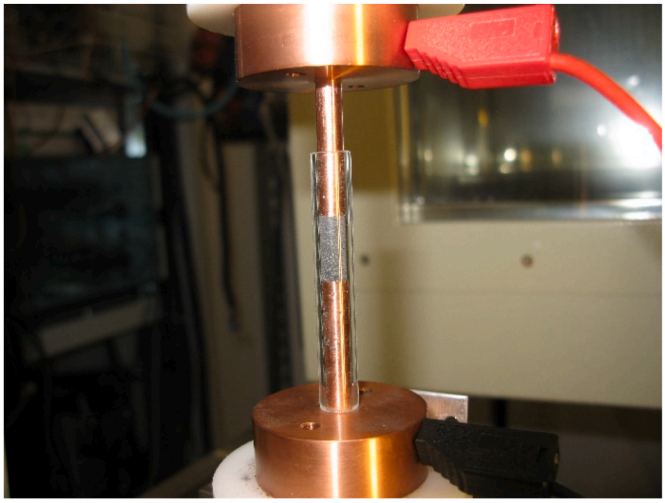

Fig. 14. Soot conductivity measurement under pressure.

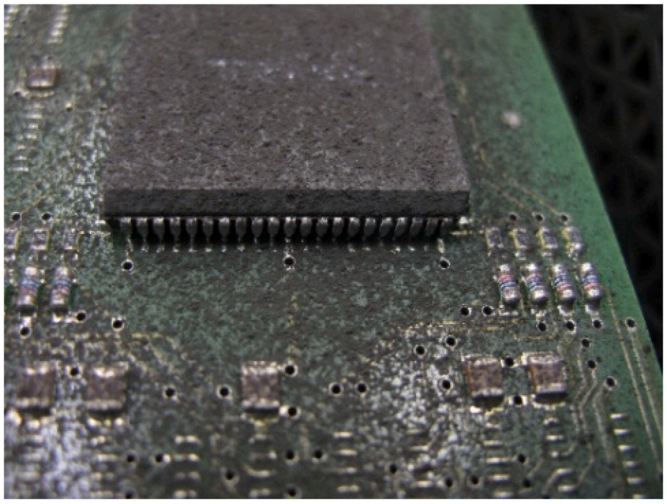

Fig. 12. Close-up of soot on printed circuit boards in PC.

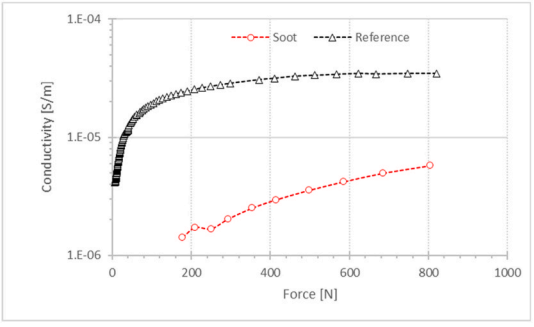

Fig. 15. Conductivity of soot on printed circuit boards compared to reference NMC sample.

Fig. 13. SEM/EDX elemental analysis of a soot sample on printed circuit boards, Nickel (left), Manganese (center), Cobalt (right).

that the heavy metals are present in the form of poorly conducting oxides.

3.2. Results sprinkling and storage water

In interpreting the contamination of sprinkling and storage water, the method of sample generation must be considered. Sprinkling water falls only on a small volume of the smoke produced during thermal runaway of the battery and is then collected in a container. A total of 280 liters of sprinkling water was collected for chemical analysis in 14 min after initiation of thermal runaway. Considering that only a small part of the smoke is sprinkled with a relatively large amount of water, the concentration of contaminants can be considered rather diluted. The burned and cooled down battery was placed in the storage container, which then was filled with approximately 50 liters of process water. The contaminants found in this were washed out by the water from the burned down battery. Since the amount of water used to rinse the battery this way is relatively small in relation to the volume of the battery (15 l), it is possible to speak of a rather high concentration in terms of contamination. The quantitative comparison of contaminations with limit and background levels in Table 13 must be seen in the light of the dilution or concentration produced. Samples for chemical analysis were taken from both containers after the entire content has been thoroughly mixed with a power tool.

3.2.1. Sprinkling water

In the sprinkling water, which has a pH value of 8 and has a moderate electrical conductivity of almost 500 µS/cm, only low levels of water-soluble sulphates (34 mg/l), fluorides (8 mg/l), chlorides and nitrates (2 mg/l each), and lithium ions (4 mg/l) were detected, see Table 10. The analyzed anion and cation levels of sulphates, chlorides and nitrates were well below the limit for drinking water in Switzerland, see Table 13. The analyzed fluoride levels exceeded the limit by a factor of five. The analyzed lithium levels exceeded the typical levels of drinking water in Germany (<0.05 mg/l) by a factor of >80 (a limit value does not exist in Switzerland).

Dissolved organic substances caused by the fire (PAH, PCB, PCDD/F) were detected only in extremely low concentrations of 1.9 µg/l (PAH; Σ 16 EPA-PAH), 0.2 ng/l (PCB; Σ 6 cong. Ballschmiter x 5) and 0.013 ng/l (PCDD/F; Σ I-TEQ), see Table 11. In the case of PCBs and PCDD/Fs, the concentrations were in the range of the process water used for sprinkling. In the case of PAHs, the dissolved amounts were 30 times higher than those found in process water. The applicable limit for drinking water were not exceeded in the case of PAHs (dissolved fractions) or were exceeded by a factor of 4–7 (particle-bound fractions). PCB concentrations were in the range of typical levels found in Swiss watercourses (dissolved and particle-bound fractions).

The heavy metals nickel, cobalt and manganese were detected in very high acid-soluble concentrations of 36 mg/l each, see Table 12. These levels exceed the limit for drinking water in Switzerland (where they are defined) by factors of 700 to 1,800, see Table 13. The limits for introducing fluids into the sewage system for industrial effluent in Switzerland are exceeded by factors of 20–70.

3.2.2. Storage water

The storage water of the battery is highly alkaline (pH 12) and has a very high electrical conductivity of about 35,000 µS/cm. The analysis found very high concentrations of water-soluble fluorides (330 mg/l) and lithium ions (1600 mg/l) in addition to low levels of water-soluble sulphates (98 mg/l), chlorides (2 mg/l) and nitrates (<1 mg/l), see Table 10. The amounts found for fluoride exceed the limit for drinking water in Switzerland by a factor of 220, see Table 13. The amounts found for lithium exceed the typical levels of drinking water in Germany (<0.05 mg/l) by a factor of >30,000 (a limit does not exist).

Organic substances caused by the fire (PAH, PCB, PCDD/F) were detected only in extremely low dissolved concentrations of 0.11 µg/l (PAH; Σ 16 EPA-PAH) and 2.9 ng/l (PCB; Σ 6 cong. Ballschmiter x 5), PCDD/F content was below detection limit, see Table 11. In the case of

Table 10
Anion and cation contamination (water samples, aqueous extract and CE), all values in mg/l.

Designation	Sample Id.	Chloride Cl^-	Fluoride F^-	Sulfate SO_4^{2-}	Ammonium NH_4^+	Potassium K^+	Sodium Na^+	Magnesium Mg^{2+}	Calcium Ca^{2+}	Lithium Li^+
Sprinkling water	W-41	2	8	34	bdl	bdl	bdl	11	67	4
Storage water	SW-41	22	330	98	16	59	52	bdl	bdl	1600
Reference, process water	0W–K	3	bdl	2	bdl	bdl	5	bdl	bdl	bdl

Table 11
Organic contamination in water samples (acidulated) and *filtrate* (suspended particles in water samples).

Designation	Sample Id.	PAH Σ16 EPA-PAH			PCB Σ 6 cong. Ballschmiter x 5			PCDD/PCDF Σ I-TEQ		
		µg/l	*µg/l*	*mg/kg*	ng/l	*ng/l*	*µg/kg*	ng/l	*ng/l*	*µg/kg*
Sprinkling water	W-43 water, *filtrate*	1.9	*1.8*	*11*	0.2	*0.67*	*4.1*	0.013	*0.032*	*0.2*
Storage water	SW-43 water, *filtrate*	0.11	*3.4*	*3.2*	2.9	*0.91*	*0.9*	bdl	*1.0*	*0.92*
Reference, process water	0W–O water	0.06	–	–	0.2	-	-	0.018	-	-

Proportions of suspended particles: W-43 = 0.16 g/l; SW-43 = 1.15 g/l.

Table 12
Nickel, Cobalt, Manganese and Lithium content in water samples (acidulated) and filtrate (suspended particles in water samples).

Designation	Sample Id.	Nickel			Cobalt			Manganese			Lithium		
		mg/l	mg/l	% by mass	mg/l	mg/l	% by mass	mg/l	mg/l	% by mass	mg/l	mg/l	% by mass
Sprinkling water	W-42 water *W-45 filtrate*	36	*48*	*22*	36	*46*	*21*	36	*44*	*20*	7	*3.1*	*1.4*
Storage water	SW-42 water *SW-45 filtrate*	55	*181*	*10*	50	*181*	*10*	53	*199*	*11*	1460	*31*	*1.7*
Reference,process water	0W- water	<0.7			<0.4			<1.3			<1.3		

Proportions of suspended particles in filtrate: W-45 = 0.22 g/l; SW-45 = 1.81 g/l.

Table 13
Comparison of contamination of sprinkling and storage water with limit and background levels.

Contaminant/ Parameter	Unit	Sprinkling water	Storage water	Process water	Drinking water limit values [1]	Industrial effluent limit value [2]
pH value	-	8.2	12.3	8	6.8 - 8.2	6.5 - 9.0
Chloride	mg/l	2	22	3	250	n.s.
Sulphate		34	98	2	250	n.s.
Nitrate		2	< 1	< 1	40	n.s.
Phosphate		<1	< 1	< 1	1	n.s.
Fluoride		8	330	< 1	1.5	n.s.
PAH [c]	µg/l	0.001 [a] 0.36 [b]	0.02 [a] 0.02 [b]	0.001 [a] < 0.001 [b]	0.1	n.s.
Benzo[a]pyrene		< 0.001 [a] 0.07 [b]	0.004 [a] 0.01 [b]	< 0.001 [a] < 0.001 [b]	0.01	n.s.
Nickel		36000 [a] 48400 [b]	55000 [a] 181000 [b]	< 700	20	2000
Cobalt		36000 [a] 46000 [b]	50000 [a] 181000 [b]	< 400	n.s. (≤ 70)	500
Manganese		36000 [a] 44000 [b]	53000 [a] 199000 [b]	< 1300	50	n.s.
Lithium		7000 [a] 2200 [b]	1460000 [a] 31000 [b]	< 1300	n.s. (≤ 40)	n.s.

[a] Content, dissolved/ [b] Content, particle-bound/ [c] Sum of Benzo[b]fluoranthene, Benzo[k]fluoranthene, Benzo[ghi]perylene, Indeno[1,2,3-cd]pyrene
[1] Limit values for drinking water in Switzerland in accordance with the Decree of the Swiss Federal Department of Home Affairs (EDI) regarding the water and drinking water in baths and shower facilities that are accessible to the public (TBDV, 2016)
[2] Discharge limit values for industrial effluent into Swiss sewage system in accordance with the Swiss Waters Protection Ordinance (GSchV) (2014)
n.s. = not specified
Color code key for the table:
green = lower than limit value for drinking water
yellow = up to 10x over the limit value for drinking water
orange = 50x to 200x over the limit value for drinking water
red = > 500x over the limit value for drinking water

Table 14
Fire soot samples on collector plates (3.5 m height), quantities and orienting element analysis with SEM/EDX, sampling area 8000 cm^2.

Distance of collector plate from fire	Sample Id.	Quantity	Composition, all samples	
50 m	C-2	0.4 g/m^2	Co, Ni, Mn	each 10–15% w/w
100 m	D-2	0.4 g/m^2	O	20–25% w/w
150 m	E−2	0.1 g/m^2	C, Ca	each 10–15% w/w
			Si, Al, Mg, S, F	each ≤ 1–5% w/w

PAHs, the dissolved amounts were in the range of the process water. In the case of PCBs, the dissolved amounts are 15 times higher than those found in process water. The applicable limits for drinking water were not exceeded in the case of PAHs (dissolved and particle-bound fractions). The amount of PCB exceeded the typical levels of Swiss watercourses (dissolved and particle-bound fractions) by a factor of 5–15.

The heavy metals nickel, cobalt and manganese were found in very high acid-soluble concentrations of 50–55 mg/l each, Table 12. This exceeds the limits for drinking water in Switzerland (where they are defined) by factors of 1000 to 2800. The limits for introducing fluids into the sewage system for industrial effluent in Switzerland are exceeded by factors of 30–100.

For sprinkling and storage water other anions (Bromide Br^-, Sulfate SO_4^{2-}, Nitrate NO_3^-, Phosphate PO_4^{3-}, Formate $HCOO^-$, Acetate CH_3COO^-) were assessed but found not to be present above the detection limit (bdl) of the respective method (<0.1 µg/cm^2) or smaller than background values measured pre experiment.

3.3. Results transport and deposition behaviour

The mixture of fire soot and construction dust resulting from the experiment was deposited in the tunnel at all measuring points in quantities of less than 0.5 g/m^2. The mixture consists of around 7–9% by mass of the elements Co, Ni and Mn, around 10–15% by mass of the elements Ca and C, around 20–25% by mass of the element O and around 1–5% by mass of the elements Si, Al, Mg, S and F, see Table 14.

Table 15
Content of metals in fire soot swipe samples by ICP-OES analysis (method A, µg/cm^2), sampling area 480 cm^2 (200 cm^2 for V-12) and direct analysis of soot with ED-XRF (*method B*, % by mass, mean value of triple measurement ± rounded up standard deviation), sampling area 8000 cm^2.

Distance from fire	Sample Id./ Method	Nickel		Cobalt		Manganese		Lithium
		A	*B*	A	*B*	A	*B*	A
50 m, collector plate	C-12, *C-2*	4.6	*7.4 ± 0.5*	4.5	*7.5 ± 0.5*	4.3	*8.3 ± 0.5*	0.8
100 m, collector plate	D-12, *D-2*	4.3	*7.4 ± 0.5*	4.3	*7.5 ± 0.5*	4.1	*8.1 ± 0.5*	0.6
150 m, collector plate	E−12, *E-2*	2.3	*7.5 ± 0.5*	2.3	*7.5 ± 0.5*	2.2	*8.0 ± 0.5*	0.3
55 m, ventilator surface	V-12	18	–	19	-	17	-	2.6

Table 16
Contamination with organic pollutants (surface swipe samples, Sohxlet extract and GC-HRMS), sampling area 1000 cm^2.

Designation	Sample Id.	PAH Σ16 EPA-PAH µg/m^2	*PCB* Σ 6 cong. Ballschmiter x 5 µg/m^2	*PCDD/PCDF* Σ I-TEQ ng/m^2
50 m	C-13, *C-14*	8.8	*0.2*	*0.2*
100 m	D-13, *D-14*	7.6	*1.1*	0.2
150 m	E−13, *E-14*	5.9	*0.18*	*0.2*
Ventilator	V13, *V14*	17	*0.66*	*0.4*

On the collector plates, the elements Co, Ni and Mn were detected at concentrations of approximately 2–5 µg/cm^2 each and elemental Li amounting to around 0.3–0.8 µg/cm^2 was found (see Table 15). On the ventilator housing (horizontal surface) Co, Ni and Mn were detected at approximately 20 µg/cm^2 each and Li was found at concentrations of around 3 µg/cm^2. Therefore, usual background levels for non-contaminated surfaces are exceeded by a factor of 50–200 (Co, Ni), 5–20 (Mn) and 10–30 (Li). Only small amounts of water-soluble chloride and bromide (≤5 µg/cm^2) and fluoride (1 µg/cm^2) were measured in all samples, which is negligible from a chemical corrosion standpoint.

The measured PAH, PCB and PCDD/F exposures of ≤10 µg/m^2 (PAH), ≤1 µg/m^2 (PCB) and <1 ng/m^2 (PCDD/F), see Table 16, are within the normal range for background levels of non-contaminated surfaces and well below restoration goals [39].

3.4. Temperature measurements

Temperatures in and around the battery in thermal runaway were measured in all three experiments and showed very similar results, see Fig. 16 as example. Here the highest temperature measured occurred at point T5 (approx. 850 °C, near battery, in the fire cone). From this maximum value, the temperature dropped below 200 °C within less than 30 s and was under 100 °C within around 100 s. The temperatures measured in the core of the battery (T1, T2) increased to over 600 °C within 173 s after detonation, corresponding to a rate of around 3.4 K/s. The maximum temperature measured in the core of the battery was 661 °C, reached after 10.3 min (T2). The temperatures in the cell stack slowly decreased from their maximum values and only fell below 200 °C after about 92 min. The highest temperature in the sidewall of the cell stack was attained after 240 s and was 617 °C (T3), although the initial temperature increase in the first 5 s was at a rate of 43.6 K/s. A maximum temperature of 395 °C was registered under the cell stack after 12 min.

The molten and subsequently solidified aluminum leaking from the battery, see Fig. 17, indicates that the temperatures in the core of the battery were higher than the melting point of aluminum, i.e. 660 °C.

4. Conclusion

Using the scalable experimental design, a contamination with soot in the range of 20 g/m^2 can be expected when a lithium-ion battery of 32 kWh capacity burns down in an enclosed parking space for 30 cars. Thermal runaway and fire of a battery of type NMC 111 produced soot consisting mainly of heavy metal-oxides of nickel, manganese and cobalt (each 18–20% by mass) as well as, to a lesser extent, of lithium (3–4% by mass), fluorides (appr. 2.5% by mass) and chlorides (appr. 0.2% by

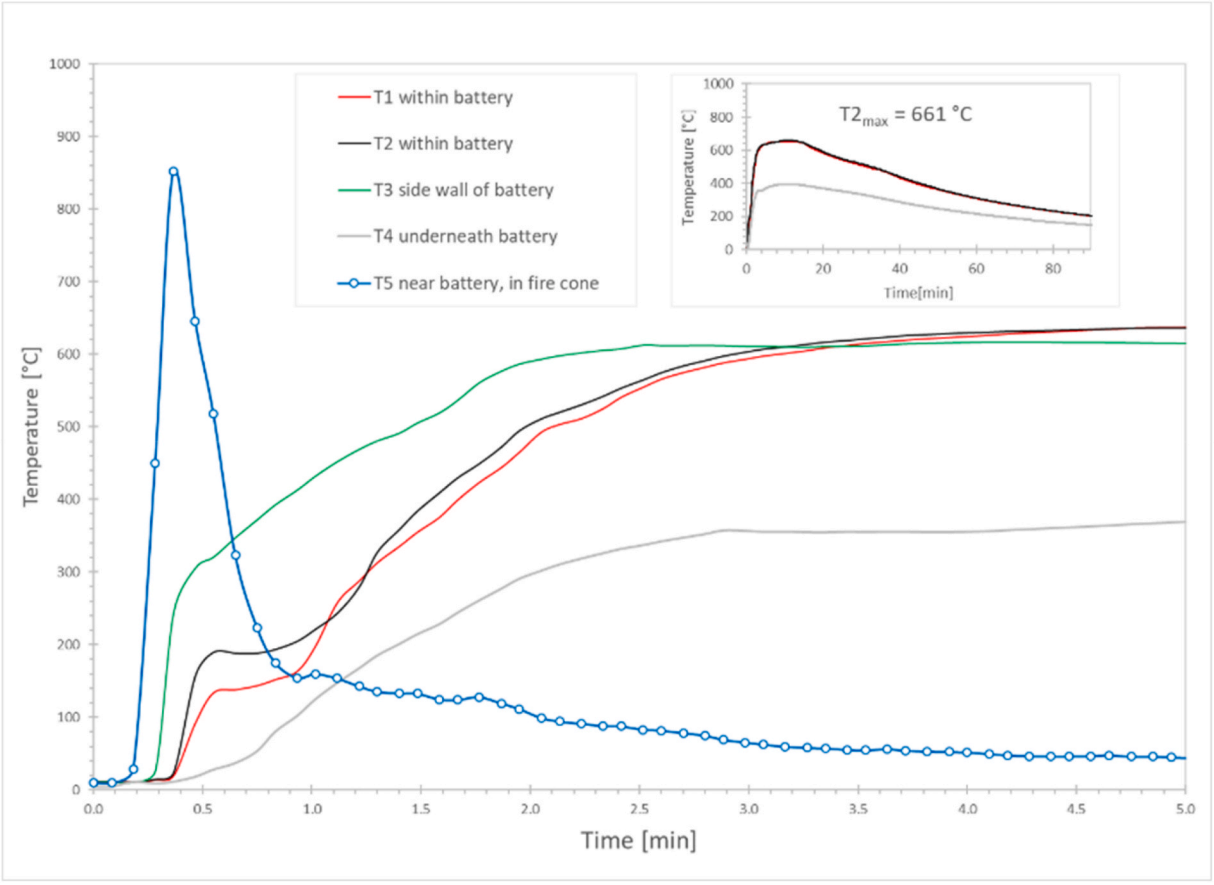

Fig. 16. Temperatures during and after thermal runaway.

Fig. 17. Molten aluminum leaked from the battery.

mass). This dry soot was found to be electrically non-conductive, even under mechanical pressure and non-corrosive, which is an important finding for the safety and the preservation of value of technical infrastructure.

With regard to toxicologically relevant organic pollutants, slightly elevated PAH quantities of approximately 250–300 μg/m^2 were detected on collector plates and 120 μg/m^2 on textiles, which exceeded the measured background levels for non-contaminated surfaces by factors up to approximately 50 and 20, respectively. The level of contamination with PAH is therefore up to a factor of three higher than the restoration goal for industrial environments.

The results of experiment 3 indicate that with active ventilation, soot is transported over long distances and is deposited on surfaces. The amounts of soot found were much lower e.g. about 0.5 g/m^2 at 100 m distance compared to 17–20 g/m^2 in the enclosed space of experiment 1. However, the quantities of the heavy metals nickel, cobalt and manganese as well as lithium are still high, which is why professional decontamination is also required here.

The analysis of sprinkling and storage water has shown that essentially the same substances are dissolved in it as occur in dry fire soot, in particular the heavy metal oxides of nickel, cobalt and manganese as well as lithium. Although the amount of contaminants found in the sprinkling and storage water is of course highly dependent on the respective dilution, it must be expected that limit values for drinking water and for industrial effluents will be massively exceeded.

5. Discussion

For the interpretation and discussion, it is important to note again that the observed results refer to the cold fire area. Effects such as the formation and decay of potentially toxic or explosive gases were not part of this study. Questions regarding decontamination, corrosion, damage to electrical or electronic equipment, and the treatment of sprinkling and storage water can be clearly identified and answered as follows:

Is the decontamination of areas/facilities after a battery fire more costly or more difficult?

After the experiments, the heavily contaminated area (test site A) was comprehensively cleaned with a standard procedure for spaces such as these i.e. professional cleaners wearing personal protective equipment. Following cleaning, all concentrations, particularly those for heavy metals and fluoride and lithium, were measured and found to be under the empirical background levels used by industry as actual target values. This also applies to textiles after a normal washing cycle. Therefore, we can assume that decontamination after a BEV fire is neither more difficult nor more costly compared to a fire of a conventional vehicle.

Does contamination caused by a battery fire lead to corrosion chemical impairment of infrastructure facilities?

The results of this investigation have clearly shown that the substances released and deposited by a battery fire are not corrosive. We can therefore expect that a BEV fire will not lead to an excessive impairment of technical infrastructure in road tunnels and enclosed parking garages compared to a fire of a conventional vehicle.

Does contamination caused by a battery fire lead to an impairment of electrical and electronic equipment?

Results show that the contamination of the battery fire consists mainly of the electrically insulating heavy metal oxides. The formation of electrically conductive paths leading to leakage currents or short circuits in electric or electronic equipment is therefore not to be expected. However, electrical impairment for plug, sliding, and switching contacts and mechanical impairment for moving parts or rotating machines must be expected as with any deposit of contamination.

Is contamination of sprinkling or storage water critical?

Yes. Results show that sprinkling water used during a battery fire as well as storage water is heavily contaminated. As the concentrations of lithium and the heavy metal oxides of cobalt, nickel and manganese massively exceed the applicable and/or currently available limit values for discharging water into the sewage system, appropriate pre-treatment of any water that was used in such battery fires (firefighting water, water from sprinkler systems, water used to store burned batteries or vehicles) must be implemented. Therefore, it is also recommended that minimum standards and guidelines for first responders regarding planning, training, procedure and equipment for chemical incidents be applied so that waste and wastewater are disposed of in an environmentally friendly and professionally correct manner.

Credit author statement

Marcel Held: Conceptualization, Methodology, Investigation, Writing – original draft Martin Tuchschmid: Conceptualization, Methodology, Investigation, Validation, Visualization Markus Zennegg: Formal analysis, Investigation, Validation, Writing – review & editing Renato Figi: Formal analysis, Investigation, Validation Claudia Schreiner: Formal analysis, Investigation, Validation Lars Derek Mellert: Conceptualization, Project administration, Writing – original draft Urs Welte: Conceptualization, Supervision, Michael Kompatscher: Conceptualization, Supervision Michael Hermann: Conceptualization, Methodology, Investigation Léa Nachef: Supervision, Validation

Funding

This research was partially supported by the Federal Roads Office of Switzerland, ASTRA (grant AGT 2018/006).

Declaration of competing interest

The authors declare that they have no known competing financial interests or personal relationships that could have appeared to influence the work reported in this paper.

Acknowledgment

We thank Günter Grossmann and Luis Caceres for performing soot conductivity measurements and SEM/EDX analysis.

Appendix A. Supplementary data

Supplementary data to this article can be found online at https://doi.org/10.1016/j.rser.2022.112474.

References

[1] OECD/ITF. The cost and efficiency of reducing transport GHG emissions. 2009.
[2] OECD/ITF. Good to go? Assessing the environmental performance of new mobility. 2020.
[3] International Council on Clean Transportation. Effects of battery manufacturing on electric vehicle life-cycle greenhouse gas emissions. 2018.
[4] International Energy Agency. Global EV outlook. May 2019.
[5] Allianz SE. The EV-olution of mobility. June 15, 2020.
[6] Li M, Lu J, Chen Z, Amine K. 30 Years of lithium-ion batteries. Adv Mater 2018. https://doi.org/10.1002/adma.201800561.
[7] Hannan Ma M, Hoque MM, Hussain A, Yusof Y, Ker PJ. State-of-the-Art and energy management system of lithium-ion batteries in electric vehicle applications: issues and recommendations. IEEE Access 2018;6:19362–78. https://doi.org/10.1109/ACCESS.2018.2817655.
[8] Blomgren GE. The development and future of lithium ion batteries. J Electrochem Soc 2017;164(1):A5019–25.
[9] Schmuch R, Wagner R, Hörpel G, Placke T, Winter M. Performance and cost of materials for lithium-based rechargeable automotive batteries. Nat Energy 2018;3:267–78. https://doi.org/10.1038/s41560-018-0107-2.
[10] Li W, Erickson EM, Manthiram A. High-nickel layered oxide cathodes for lithium-based automotive batteries. Nat Energy 2020;5:26–34. https://doi.org/10.1038/s41560-019-0513-0.
[11] Kim J, Lee H, Cha H, Yoon M, Park M, Cho J. Prospect and reality of Ni-rich cathode for commercialization. Adv Energy Mater 2018;8. https://doi.org/10.1002/aenm.201702028.
[12] Wang X, Ding YL, Deng YP, Chen Z. Ni-Rich/Co-Poor layered cathode for automotive Li-ion batteries: promises and challenges. Adv Energy Mater 2020;10. https://doi.org/10.1002/aenm.201903864.
[13] pushevs.com [Internet]. [redacted]
[14] Bisschop R, Willstrand O, Amon F, Rosengren M. RISE research institutes of Sweden AB. Fire safety of lithium-ion batteries in road vehicles. RISE Report 2019:50.
[15] Hendricks C, Williard N, Mathew S, Pecht M. A failure modes, mechanisms, and effects analysis (FMMEA) of lithium-ion batteries. J Power Sources 2015;297:113–20.
[16] Wang Q, Ping P, Zhao X, Chu G, Sun J, Chen C. Thermal runaway caused fire and explosion of lithium ion battery. J Power Sources 2012;208:210–24. https://doi.org/10.1016/j.jpowsour.2012.02.038.
[17] Li H, Duan Q, Zhao C, Huang Z, Wang Q. Experimental investigation on the thermal runaway and its propagation in the large format battery module with Li($Ni_{1/3}Co_{1/3}Mn_{1/3}$)O_2 as cathode. J Hazard Mater 2019;375:241–54. https://doi.org/10.1016/j.jhazmat.2019.03.116.
[18] Gao S, Lu L, Ouyang M, Duan Y, Zhu X, Xu C, Ng B, Kamyab N, White RE, Coman PT. Experimental study on module-to-module thermal runaway-propagation in a battery pack. J Electrochem Soc 2019;166(10):A2065–73. https://doi.org/10.1149/2.1011910jes.
[19] Golubkov AW, Planteu R, Krohn P, Rasch B, Brunnsteiner B, Thaler A, Hacker V. Thermal runaway of large automotive Li-ion batteries. RSC Chem 2018;8:40172–86. https://doi.org/10.1039/c8ra06458j.
[20] Li H, Chen H, Sun J, Wang Q, Peng W, Yang X. Full-scale experimental study on the combustion behavior of lithium ion battery pack used for electric vehicle. Fire Technol 2020;56:2545–64. https://doi.org/10.1007/s10694-020-00988-w.
[21] Federal Aviation Administration. Lithium battery thermal runaway vent gas analysis. 2016. DOT/FAA/TC-15/59.
[22] Roth EP, Crafts CC, Doughty DH, McBreen J. Advanced Technology development program for lithium-ion batteries: thermal abuse performance of 18650 Li-ion cells. Sandia National Laboratories; 2004. SAND2004-0584.
[23] Li W, Wang H, Zhang Y, Ouyang M. Flammability characteristics of the battery vent gas: a case of NCA and LFP lithium-ion batteries during external heating abuse. J Energy Storage 2019;24. https://doi.org/10.1016/j.est.2019.100775.
[24] Golubkov AW, Fuchs D, Wagner J, Wiltsche H, Stangl C, Fauler G, Voitic G, Thaler A, Hacker V. Thermal-runaway experiments on consumer Li-ion batteries with metal-oxide and olivin-type cathodes. RSC Adv 2014;4:3633. https://doi.org/10.1039/c3ra45748f.
[25] Kunkelmann J. Untersuchung des Brandverhaltens von Lithium-Ionen- und Lithium-Metall-Batterien in verschiedenen Anwendungen und Ableitung einsatztaktischer Empfehlungen. Forschungsbericht Nr. 175. German: Karlsruher Institut für Technologie (KIT) Forschungsstelle für Brandschutztechnik; 2015.
[26] Campion CL, Li W, Lucht BL. Thermal decomposition of $LiPF_6$-based electrolytes for lithium-ion batteries. J Electrochem Soc 2005;152(12):A2327–34. https://doi.org/10.1149/1.2083267.
[27] Eshetu GG, Bertrand JP, Lecoq A, Grugeon S, Laruelle S, Armand M, Marlair G. Fire behavior of carbonates-based electrolytes used in Li-ion rechargeable batteries with a focus on the role of the $LiPF_6$ and LiFSI salts. J Power Sources 2014;269:804–11. https://doi.org/10.1016/j.jpowsour.2014.07.065.
[28] Ribière P, Grugeon S, Morcrette M, Boyanov S, Laruelle S, Marlaair G. Investigation on the fire-induced hazards of Li-ion battery cells by fire calorimetry. Energy Environ Sci 2012;5:5271. https://doi.org/10.1039/c1ee02218k.
[29] Larsson F, Andersson P, Blomqvist P, Mellander BE. Toxic fluoride gas emissions from lithium-ion battery fires. Sci Rep 2018;8(1):5265. https://doi.org/10.1038/s41598-017-09784-z.
[30] Lecoq A, Eshetu GG, Grugeon S, Martin N, Laruelle S, Marlair G. Scenario-based prediction of Li-ion batteries fire-induced toxicity. J Power Sources 2016;316:197–206. https://doi.org/10.1016/j.jpowsour.2016.02.090.
[31] Sun J, Li J, Zhou T, Yang K, Wei S, Tang N, Dang N, Li H, Qiu X, Chen L. Toxicity, a serious concern of thermal runaway from commercial Li-ion battery. Nano Energy 2016;27:313–9. https://doi.org/10.1016/j.nanoen.2016.06.031.
[32] Lecoq A, Bertana M, Truchot B, Marlair G. Comparison of the fire consequences of an electric vehicle and an internal combustion engine vehicle. 2. In: International conference on fires in vehicles - FIVE 2012; Sep. 2012. p. 183–94. Chicago, United States Ineris-00973680.
[33] Sun P, Huang X, Bisschop R, Niu H. A review of battery fires in electric vehicles. Fire Technol 2020;56:1361–410. https://doi.org/10.1007/s10694-019-00944-3.
[34] Mellert LD. Elektromobilität und Tunnelsicherheit – gefährdungen durch Elektrofahrzeugbrände. Forschungsbericht Nr. 1630. German: Federal Roads Office FEDRO; 2018.
[35] Bravo Diaz L, He X, Hu Z, Restuccia F, Marinescu M, Varela Barreras J, Patel Y, Offer G, Rein G. Meta-review of fire safety of lithium-ion batteries: industry challenges and research contributions. J Electrochem Soc 2020;167:090559. https://doi.org/10.1149/1945-7111/aba8b9.
[36] Blum AF, Long Jr RT. Fire hazard assessment of lithium ion battery energy storage systems. New York: Springer; 2016. https://doi.org/10.1007/978-1-4939-6556-4.
[37] Mellert LD, et al. Risk minimisation of electric vehicle fires in underground traffic infrastructures. Research project AGT 2018/006 petitioned by the Tunnel Research Working Group (Arbeitsgruppe Tunnelforschung, AGT). Schweizerischer Verband der Strassen- und Verkehrsfachleute (VSS). 2020. [redacted]
[38] Hu X, Yuan H, Zou C, Li Z, Zhang L. Co-estimation of state of charge and state of health for lithium-ion batteries based on fractional-order calculus. IEEE Trans Veh Technol 2018;67(11). https://doi.org/10.1109/TVT.2018.2865664.
[39] Gesamtverband der Deutschen Versicherungswirtschaft e.V. (GDV). Richtlinien zur Brandschadensanierung. Publikation zur Sach-Schadensanierung, VdS 2357: 2014-06 (06). Germany: VdS Schadenverhütung GmbH; 2014.